Title

"Phenomenological prediction of desalination brines nanofiltration through the indirect determination of zeta potential"

Authors: Ortiz-Albo, P., Ibañez, R., Urtiaga, A.M., Ortiz, I.

Affiliation: Department of Chemical and Biomolecular engineering. University of Cantabria

Address: Av. de Los Castros s/n. 39005 Santander. Spain

E-mail: urtiaga@unican.es

Submitted to

Separation and Purification Technology

April 2018

Abstract

The prediction of nanofiltration (NF) performance at environmentally relevant conditions, e.g.: highly saline brine solutions, is becoming of increasing interest for the recovery of waste materials in the water desalination industry. In this work, the prediction of the separation of sulfate and chloride contained in the retentate of reverse osmosis brackish water desalination by means of the commercial NF270 membrane is studied. Prior to theoretical modelling, streaming potential measurements were performed for aqueous single and binary mixtures of NaCl and Na_2SO_4 within the range of ionic strengths 0.001-0.1 M. Zeta potential values were obtained applying an extrapolation method from recent literature to allow the calculation of surface charge density under higher ionic strengths found in reverse osmosis desalination brines (0.1 to 1.2 M). The obtained surface charge density was then used to simulate sulfate, chloride and sodium rejections by means of the Donnan steric pore model (DSPM), in the pressure range 2 – 20 bar. The good agreement between experimental and simulated rejection values allows to validate this approach that enables the prediction of NF performance for the separation of monovalent and divalent anions, of interest for the purification of desalination brines before their further exploitation as a source of sodium chloride concentrated solutions.

Keywords: nanofiltration, NF270, zeta potential, desalination brines, Donnan-steris-pore model

1. Introduction

Nanofiltration (NF) separation relies both on the pore size and on the surface charge properties of the membrane. While the large molecules are retained because of the small pore size, which is usually lower than 1 nm in diameter, smaller charged species can be also rejected as a result of the electric repulsion effect exerted by the charged surface of the membrane. Negatively charged NF membranes are particularly effective for the rejection of multivalent ions, such as sulfate and calcium [1–4]. Compared to reverse osmosis (RO), NF offers higher permeate fluxes at moderate operation pressure, making it the preferred option for the treatment of moderately salty water, as it the case of brackish groundwater [5–9]. Also, examples of the increasing relevance of NF in applications involving high salinity solutions can be found in the pre-treatment in RO seawater desalination [10,11], and by its integration in material recovery processes from RO desalination brines to be reused in several chemicals manufacturing processes, e.g.: chlorine production by electrolysis [12], conversion of NaCl into hydrochloric acid and sodium hydroxide by means of bipolar membrane electrodialysis [13–16].

The understanding of separation phenomena in NF membranes has been of interest in the last decades, fostering the development of novel experimental methods [17] and mathematical models with moderately good predictive capability [18]. The typical approach of these models is essentially based on the extended Nernst-Planck (ENP) equation, which best fulfills the transport of ions across the membrane in terms of diffusion, electromigration and convection [3,19,20]. Other alternative for NF modeling is the Spiegler-Kedem (SK) model [21–23], which considers the NF membrane as a black box, to fit experimental data in terms of two parameters, salt permeability and reflection coefficient. The SK model is characterized by its simplicity and has properly predicted the rejection of single multivalent salts [22] and high saline mixtures [24] containing sodium chloride and magnesium chloride or sodium sulfate near their concentration in seawater. However, neither the detailed physical phenomena nor the membrane characteristics are considered by the SK model.

With regard to the use of the ENP equation, different phenomena have been included in order to achieve greater accuracy and predictive capability giving rise to a number of suitable models, which mainly differ in their strictness and complexity [18,19,25–29]. The inclusion of the Donnan [19] and steric effects [30] in the liquid-membrane

interfaces, derived in the Donnan-Steric-Pore-Model (DSPM). Further studies [31,28] included the dielectric exclusion (DE) in the DSPM, emerging the DSPM&DE model.

The overwhelming amount of approaches for predictive models are mostly thought to be applied under diluted and idealized solutions, composed of only 2, 3 or sometimes 4 ions. The application of these models to describe NF performance under realistic industrial conditions is far from accurate when concentrated multi-component solutions are considered. Added to this, the accurate characterization of NF membranes parameters has been widely discussed in previous studies [1,17,25,26,31,32] as one of the main challenges to face in the modelling of this technology.

NF membranes, as semipermeable membranes, acquire a surface charge when they are in contact with aqueous solutions through several possible mechanisms, among which the most relevant ones are the dissociation of the functional groups included in the polymer material forming the top surface, and the adsorption of ions and charged macromolecules from the solution. Several theories have discussed the spatial distribution and concentration of ionic species in solution induced by the membrane surface charge [20,33,34]. The most complete and realistic theory, that has been followed in this study, is the formation of an electric double layer (EDL), which assumes a fixed layer of charges at the surface of the membrane, and a layer of mobile charges in the liquid layer adjacent to the membrane. Accordingly, one recent study [33] discussed the zeta potential determination and surface charge behaviour of forward osmosis (FO) membranes when high ionic strengths were considered. The research work of Coday et al. [33] disagreed with the commonly accepted assumption of neutralization of the membrane charge at high ionic strengths and established that the neutralization was not achieved; instead, a constant value of zeta potential was reached, due to the limitation of the compression of the diffusive layer by the size of the ions involved.

Considering this background, the present study is focused on the prediction of the commercial NF270 membrane performance in the nanofiltration of highly concentrated mixtures of divalent (sulfate) and monovalent (chloride) anions, and particularly in the estimation of the charge density developed by the membrane when it is in contact with concentrated salts solutions, by means of streaming potential measurements. The extrapolation method developed by Coday et al. [33] will be applied. The validity and accuracy of the prediction will be assessed by the comparison of theoretical calculations

and experimental results of the NF270 performance in the separation of mixed sulfate (0.2 to 1.2 M) and chloride (1.0 M) solutions reported in the case study [3]. The motivation of this work comes from the interest in the recovery of monovalent ions, Cl^- and Na^+, from RO water desalination brines, which contain not only NaCl but also other species that interfere with the above-mentioned recovery by reducing the quality of products. Among others, sulfate anion is commonly encountered in RO brines, particularly in inland brackish water desalination operations.

2. Theoretical background

The NF model applied in this work is the Donnan Steric Pore Model (DSPM) [19], as it was applied in a previous study [3]. DSPM enables a comprehensive mathematical description to gain insight into the separation mechanism of nanofiltration membranes, providing the tools for process design and optimization.

The equations considered in the model are summarized in Table 1, and take into account the ions transport through the membrane (Eq. 12), along with steric (Eq. 18) and Donnan effects in equilibrium partitioning at interfaces: feed/membrane (Eq. 9) and membrane/permeate (Eq. 10), as well as the hindered nature of diffusion and convection phenomena inside the pores (Eq. 16-17). Equations for mass balances at steady state (Eq. 1-3) and polarization of feed concentration (Eq. 11) are included in the model. The parameters needed for the description of concentration polarization phenomena at the liquid layer adjacent to the membrane, e.g.: mass transfer coefficients, osmotic pressures, and the membrane permeability were obtained from the literature [3].

Experimental data, which were taken from our previous study [3], were obtained in a laboratory scale SEPA-CF (GE Osmonics, France) cross-flow module, provided with a flat NF270 (Dow Filmtec) membrane. The feed was pressurized at three operating pressures, 500, 1000 and 2000 kPa, and flowed at 2.5 $L \cdot min^{-1}$.

The model includes three parameters related to the membrane properties: the pore radius (r_p), the effective membrane thickness (δ) and the effective membrane charge density (X_d). The accurate knowledge of these parameters represents one of the major limitations of NF modelling and therefore, they stand as the requirement of scientific and technological progress for prediction of NF performance.

Table 1. Equations considered for DPSM predictive model.

Mass balances

$$Q_F = Q_R + Q_P \quad (1)$$

$$C_{Fi} \cdot Q_F = C_{Ri} \cdot Q_R + C_{Pi} \cdot Q_P \quad (2)$$

$$Q_P = J_v \cdot A \quad (3)$$

$$J_v = L_p \cdot (\Delta P - \Delta\pi) \quad (4)$$

$$L_p = L_{pw} \cdot \exp(-C_{eq}) \quad (5)$$

$$C_{eq} = \frac{1}{2} \cdot \sum_{i=1}^{n} |z_i| \cdot C_{Fi} \quad (6)$$

$$\pi = \frac{(T_f^* - T_f) \cdot \Delta H_f^* \cdot T}{V_{molar\ solvent} \cdot T_f \cdot T_f^*} \cdot \left[\frac{R_{pressure}}{R}\right] \quad (7)$$

$$\xi = \frac{(T_f^* - T_f)}{1.86} \cdot 1000 \quad (8)$$

Equilibrium partitioning of species at interfaces: feed/membrane and membrane/permeate

$$\frac{C_{1i}}{C_{oi}} = \phi_i \cdot \exp[-z_i \cdot \Delta\psi_{Donnan}(0)] \quad (9)$$

$$\frac{C_{2i}}{C_{Pi}} = \phi_i \cdot \exp[-z_i \cdot \Delta\psi_{Donnan}(\delta)] \quad (10)$$

Concentration polarization at feed side

$$\frac{C_{oi} - C_{Fi}}{C_{Fi} - C_{Pi}} = \exp\left(\frac{J_v}{k_i}\right) \quad (11)$$

Solute transport through the membrane

$$J_{si} = J_v \cdot K_{ci} \cdot C_i - D_{pi} \cdot \frac{dC_i}{dx} - z_i \cdot C_i \cdot D_{pi} \cdot \frac{F}{R \cdot T} \cdot \frac{d\psi}{dx} \quad (12)$$

$$\frac{d\psi}{dx} = \frac{\sum_{i=1}^{n} z_i \cdot \left(J_v / D_{pi}\right) \cdot [K_{ci} \cdot C_i - C_{Pi}]}{\left(F / R \cdot T\right) \sum_{i=1}^{n} z_i^2 \cdot C_i} \quad (13)$$

$$J_{si} = J_v \cdot C_{Pi} \quad (14)$$

$$D_{pi} = K_{di} \cdot D_{\infty i} \quad (15)$$

Hindrance factors ($0 < \lambda \leq 0.8$)

$$K_{di} = 1.0 - 2.30 \cdot \lambda_i + 1.154 \cdot \lambda_i^2 + 0.224 \cdot \lambda_i^3 \quad (16)$$

$$K_{ci} = 1.0 + 0.054 \cdot \lambda_i - 0.988 \cdot \lambda_i^2 + 0.441 \cdot \lambda_i^3 \quad (17)$$

Steric partitioning

$$\phi_i = (1 - \lambda_i)^2 \quad (18)$$

$$\lambda_i = \frac{r_i}{r_p} \quad (19)$$

Electroneutrality conditions

$$\sum_{i=1}^{n} z_i \cdot C_{Pi} = 0 \quad (20)$$

$$\sum_{i=1}^{n} z_i \cdot C_{Ri} = 0 \quad (21)$$

$$\sum_{i=1}^{n} z_i \cdot C_i + X_d = 0 \quad (22)$$

Pore radius and effective membrane thickness characterization [18,20,35] has been discussed in the literature, including gas adsorption-desorption techniques, atomic force

microscopy (AFM), scanning electron microscopy (SEM), reverse surface impregnation coupled with transmission electron microscopy (TEM) and, the most commonly used, estimation by fitting neutral solute rejection data to simulated data with NF mathematical models [25]. Lin et al. [36] selected glucose, sucrose and raffinose for NF270 pore size characterization and estimated its average pore radius as 0.54 nm. Other studies [31,37] used glucose and glycerol, resulting in r_p = 0.43 nm, which is similar to the value reported by Nghiem et al. [38], 0.42 nm. On the other hand, Hilal et al. [39] applied AFM for surface characterisation to determine the pore size distribution and the surface roughness of several NF membranes. The average r_p value for NF270 was 0.35 nm. The effective membrane thickness is usually reported as thickness to porosity ratio [37,40], which makes difficult the gathering of data and comparison of the results obtained with different characterization techniques. However, Freger [41] determined the dry thickness of NF270 by AFM (δ = 14 nm) and Pérez et al. [3] characterized it by SEM images (δ = 7 nm).

While pore radius and dense layer membrane thickness are physical membrane properties, the effective charge density depends on the interaction between the charged membrane and the electrolyte. Several approaches have been followed in previous studies [25,30]. Bowen and Mukhtar [19] considered that the main mechanism involved in the formation of surface charge is the co-adsorption of the ions onto the membrane surface. As a result, the effective charge density was related to the ions bulk concentration using the Freundlich isotherm. This assumption has been broadly accepted by several authors [1,19,25,40,42–44] for different NF membranes, including NF270. The interest of applying the Freundlich isotherm for describing effective charge density relies on its practical usefulness. However, its application in previous works has been limited to low ion concentrations.

The effective charge density is widely determined by means of electro-kinetic measurements [1,3,29,32,43,45,46]. The tangential streaming potential technique is defined as the measurement of the electrical potential difference at zero applied current, generated when a hydrodynamic pressure is applied to the electrolyte solution forcing it to flow through a capillary channel [20,25,34]. The model of the electrochemical double layer defines the zeta potential (ζ) as the electrical potential at the shear plane that separates the stationary layer and the mobile layer of charges. The zeta potential (ζ) is given by the Helmhotz-Smoluchowski (H-S) equation (Eq. 23). This parameter is strongly dependent on the pH, the ionic strength and the composition of the solution in

contact with the membrane [1,3,18,25,35,47–50]. The higher the ionic feed concentration is, the larger the effective charge density is obtained [2,19,51] due to the compression of the electrical double layer. Even so, the interest of using zeta potential is supported by practical reasons since it can relate experimental measurements of streaming potential to the surface charge density.

The surface charge density (σ_k) can be calculated by the Gouy-Chapman equation (Eq. 24). σ_k can be converted into concentration assuming that the membrane surface charge is uniformly distributed in the void volume of cylindrical pores, giving as result the effective membrane charge density (X_d) (Eq. 27) [1].

$$\zeta = \frac{dU}{dP} \cdot \frac{\eta}{\varepsilon \cdot \varepsilon_0} \cdot k \tag{23}$$

$$\sigma_k = \frac{2 \cdot \varepsilon \cdot k_B \cdot T}{z \cdot e \cdot \kappa^{-1}} \cdot \sinh\left(\frac{z \cdot e \cdot \zeta}{2 \cdot k_B \cdot T}\right) \tag{24}$$

where κ^{-1} is the Debye length of the diffuse layer following the EDL approach, calculated by Eq. 25. The ionic strength (I) of the feed solution influences the calculation of the Debye length, Eq. 26. At higher ionic strength, the Debye length decreases, which is assumed to correspond to the extension of the charges in the diffuse layer, and accelerates the shielding of the membrane charge by counter ions.

$$\kappa^{-1} = \sqrt{\frac{\varepsilon \cdot R \cdot T}{2 \cdot F^2 \cdot I}} \tag{25}$$

$$I = \frac{1}{2} \cdot \sum_i z_i^2 \cdot c_i \tag{26}$$

$$X_d = \frac{2 \cdot \sigma_k}{r_p \cdot F} \tag{27}$$

However, it is well known that the streaming potential experimental technique is not reliable when high ionic strengths are considered. Thus, Coday et al. [33] presented an indirect method for the determination of zeta potential developed by surfaces in contact with high ionic strength solutions. In the methodology developed by Coday et al. [33], the streaming potential measurements and the Debye length, at low ionic concentrations, were linearly fitted, and this behaviour was transposed to high ionic strengths. This assumption is based on the affinity of the membrane for electrostatic charge shielding when higher ion concentrations are considered, which reduces the diffuse layer as the ionic strength of the bulk solution is increased (Eq. 25). However, as it was initially

predicted by Lyklema [52], and is well known the limitation of Gouy-Chapman theory, the compression of the diffuse layer is limited by the size of the hydrated ions.

3. Materials and methods

3.1. NF membrane

A commercial nanofiltration membrane, NF270 (Dow FILMTEC) was used in this study. NF270 is a thin film composite (TFC) membrane formed by a polyester support matrix, a microporous polysulfone interlayer, and a semi-aromatic polypiperazine amide dense layer, with end groups of secondary amine (=NH) and carboxylic acids [31,36]. The surface of the NF270 membrane is negatively charged at neutral pH. Since NF270 is a widely studied commercial membrane [3,18,25,44,53], some properties needed for predictive modelling have been taken from other studies, as the average pore radius (r_p = 0.43 nm [31]) and the effective membrane thickness (δ = 7 nm [3]).

3.2. Chemistry of solutions

Sodium chloride and sodium sulfate were used to prepare aqueous salt solutions in ultrapure water (MilliPore). The concentration of sulfate was fixed at 0.056 M, and chloride concentration was varied in the range 0.085 M to 0.684 M. The concentration of salts reproduced the composition of reverse osmosis brines obtained in inland brackish water desalination, as reported in previous works [3,10, 44,54].

Based on these stock solutions, dilutions were prepared as described in Table 2, to meet the conditions for using the electrokinetic analyzer, that is, to fix the ionic strength within the range 0.1 M - 0.001 M.

3.3. Electrokinetic analyser

Streaming potential measurements were performed in the commercial electrokinetic analyzer UAnton (SurPASS, Anton Paar). Two film specimens of the NF270 membrane with dimensions 20 x 10 mm^2 were mounted, face-to-face, within the SurPASS adjustable-gap cell. The cell was inserted in the electrokinetic analyser and the system was flushed with ultrapure water for approximately 2 minutes, drained and then flushed twice with the electrolyte solution. Flow check through the adjustable gap cell was performed before each measurement after replacement of the electrolyte solution, so linear relationship between volumetric flow and pressure through the gap cell was obtained. Streaming potential measurements were performed at 25 °C and a pH of 5.3

(unless otherwise stated), using an average gap height of 105±5 μm and working at a pressure drop of the fluid through the cell of 200 mbar [34,55]. HCl 0.1 M and NaOH 0.1 M were added for pH adjustment. Each reported value of streaming potential was calculated as the average of two replicate membrane specimens. Moreover, for each membrane specimen, eight measurements of the streaming potential were taken under the same conditions (four measurements with solutions flowing from left to right and four from right to left). The conductivity and pH were measured with the probes fitted in the equipment. Besides, the dielectric constant and the viscosity of the solutions were provided by the software of the UAnton electrokinetic analyser.

Table 2. $NaCl/Na_2SO_4$ solutions prepared for streaming potential measurements.

Stock Solution	Dilution	[NaCl] (mol/m^3)	[Na_2SO_4] (mol/m^3)	I (mol/m^3)
M1	1:2	43.0	28.0	127.0
	1:10	8.60	5.60	25.4
	1:100	0.86	0.56	2.5
M2	1:10	25.70	5.60	42.5
	1:100	2.57	0.56	4.3
M3	1:10	51.30	5.60	68.1
	1:100	5.13	0.56	6.8
M4	1:10	68.40	5.60	85.2
	1:100	6.84	0.56	8.5

4. Results and discussion

4.1. Isoelectric point determination

Initial experiments were aimed at determining the zeta potential developed by the NF270 membrane for solutions of the single salts NaCl and Na_2SO_4. Streaming potential data were converted to zeta potential making use of the H-S equation (Eq. 23). Figure 1 shows the variation of the zeta potential with pH for the two electrolytes, and the following concentrations: 0.1/0.01/0.001 M NaCl and 0.01/0.001 M Na_2SO_4.

As observed in Figure 1, isoelectric points (IEP) (values of pH at which membrane zeta potential is equal to zero) were very similar for all concentrations tested and the type of electrolyte did not exert a significant influence on this membrane characteristic. Global IEP for each electrolyte was calculated as the average of IEP obtained for the different

concentrations considered for each electrolyte, giving as result: IEP (NaCl) = 3.27 ± 0.20, and IEP) = 2.99 ± 0.06 for Na_2SO_4. The IEP values experimentally determined in this work are consistent with previous studies that reported IEP of the NF270 membrane in the range 3 – 4.05 for NaCl for concentrations between 0.05 – 0.001 M [31,46,56,57].

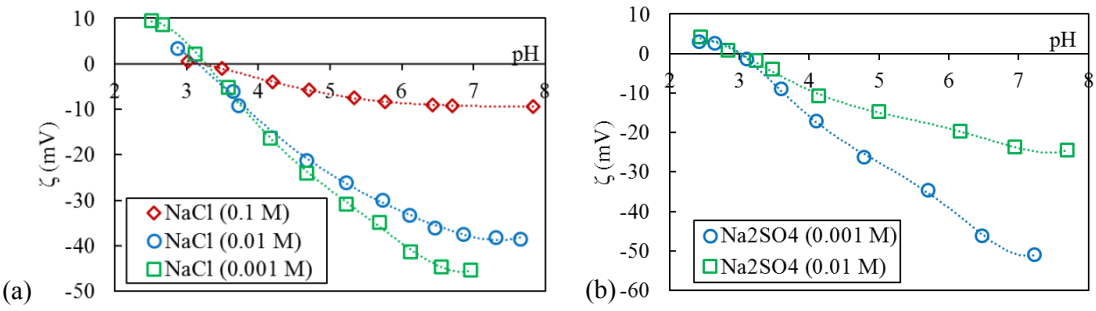

Figure 1. Zeta potential of NF270 membrane in the pH range 2.5–8.0: (a) for sodium chloride solutions, and (b) for sodium sulphate solutions.

Both electrolytes showed negative zeta potential for values of pH higher than IEP, and positive above this value. As it was discussed in previous studies that used the NF270 membrane in the range of pH 7.9-9 that is relevant for the present study, as it is typically found in reverse osmosis brines [3], the carboxyl and/or sulfonic membrane functional groups are dissociated resulting in a negatively charged membrane. The similar IEPs developed by the NF270 membrane with the two electrolytes, NaCl and Na_2SO_4, and for different electrolyte concentrations are attributed to similar dissociation of the membrane functional groups with both electrolytes. And which is more important, this behaviour gives the opportunity to work with mixtures of both electrolytes, making easier the characterization of the membrane performance when both electrolytes co-exist.

4.2. Effective Charge Density determination for high salinity solutions

Streaming potential and conductivity were measured for dilutions prepared from the different model stock solutions with different chloride/sulfate ratio, as shown in Table 2. Figure 2 shows, in a double logarithm scale, values of streaming potential plotted against the reverse of the square root of the conductivity. It is observed that the linear behaviour is common to all the measurements, independently of the differences of the chloride/sulfate ratio in each of the stock solutions. The experimental streaming potentials

at equal conductivity values presented standard deviations lower than 0.0002%. This linear regression (Eq. 28 given in the insert of Figure 2) can be used in the estimation of the streaming potential of the NF270 membrane in high salinity conditions and, therefore, zeta potential values.

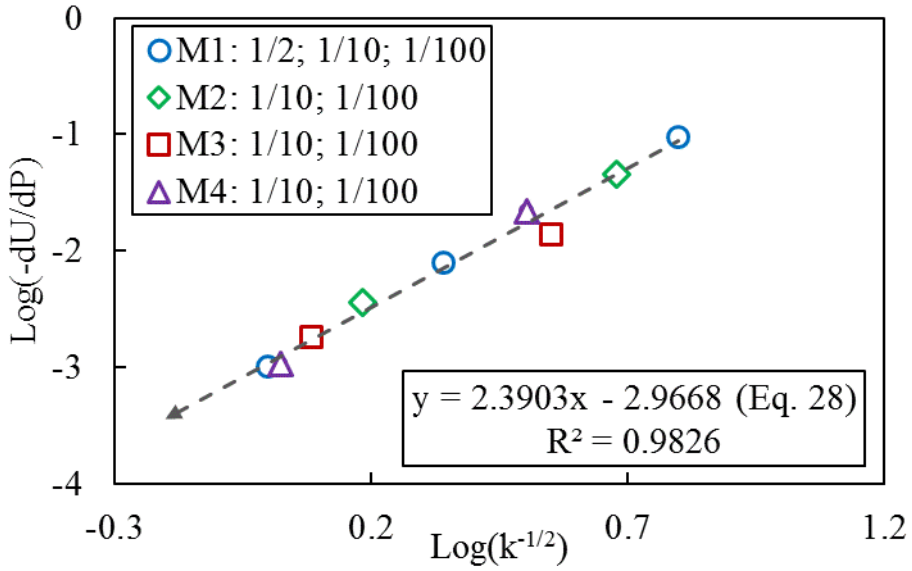

Figure 2. Log of streaming potential (mV/mbar) vs. Log of inverse square root of the conductivity ((S/m)$^{-1/2}$). Data match the linear equation (Eq. 28) provided in the figure.

Figure 3 shows the membrane zeta potential as a function of the ionic strength of the electrolyte solution. ZP calculations were accomplished using H-S approach as described in the introduction, and following the indications of the reference [33]. Blue open points represent experimental data obtained for electrolytes with ionic strengths in the range 1-100 mol/m^3, while green solid points correspond to ZP values calculated using Eq. 28, in the range of ionic strengths 100-1,200 mol/m^3. Two sections can be clearly distinguished in Figure 3. At the low range of ionic strength of the bulk solution, the membrane zeta potential becomes less negative as the ionic strength is increased. However, when the ionic strength surpasses 200 mol/m^3, the ZP values calculated from Eq. (28) take an asymptotic trend, so the extent of the diffusive layer compression is approaching its limit.

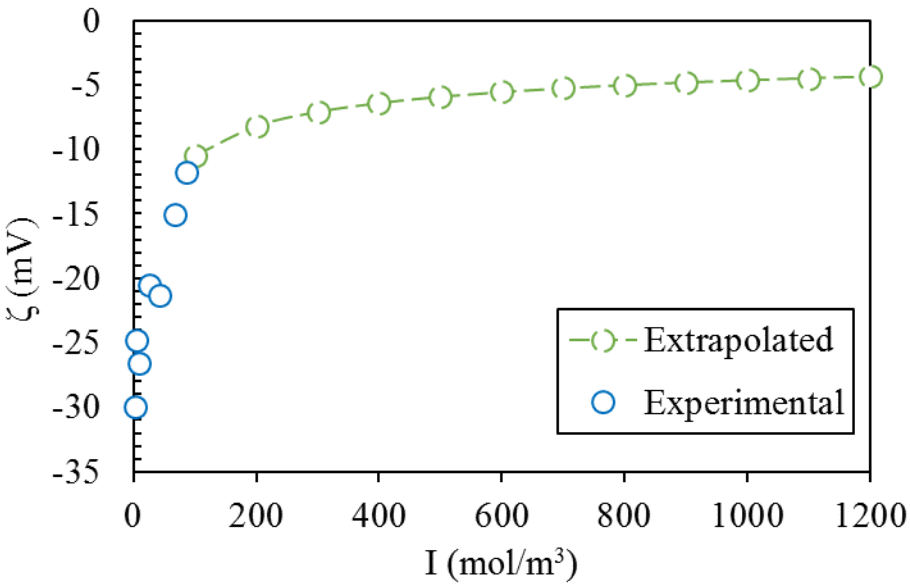

Figure 3. Zeta potential values of experimental measurements and the results of the extrapolation method applied through the range of ionic strengths of reverse osmosis brines reported by [3].

Coday et al. [33] related this performance to the size of the hydrated counter-ions that build the electrostatic shield at the diffusive layer adjacent to the charged membrane surface. ZP is determined at the surface of shear, the limit between fixed and diffusive layers, and is limited by the hydrated size of the ions. They also pointed that the value of ionic strength in which zeta potential becomes constant is equal to the value of ionic strength which gives a Debye length equal to the hydrated radius of the counter ions, calculated by Eqs. 25-26. In the present study, the membrane surface is negatively charged, and the counter ion is sodium. The ionic strength at which the zeta potential gained a practically constant value was between 1,100 and 1,200 mol/m^3, as it is depicted in Figure 3, corresponding to a Debye length of 2.76-2.88 Å. These values are in close agreement with the hydrated radium of sodium, 2.76 Å [58], which demonstrates that the diffusive layer compression is limited by the size of the hydrated counter - ion, as it was proposed by Coday et al. [3]. Therefore, higher ionic strength than 1,200 mol/m^3 should not be used in this method. Pérez-González et al. [3] considered that at high salinity, the zeta potential could be assumed to be constant, which is not far from the extrapolated results reported in this work (Figure 3).

Next, the effective charge density developed by the NF270 membrane in contact with the different brine solutions was calculated using Eq. (28) that serves to extrapolate streaming potential values at higher ionic strengths that those used in the experimental measurements. Figure 4 shows with a dotted line the simulation of the charge density obtained for ionic strengths in the range from 100 to 1,200 mol/m^3. The ionic strengths that correspond to the brine solutions (M1 to M4) are marked as filled symbols.

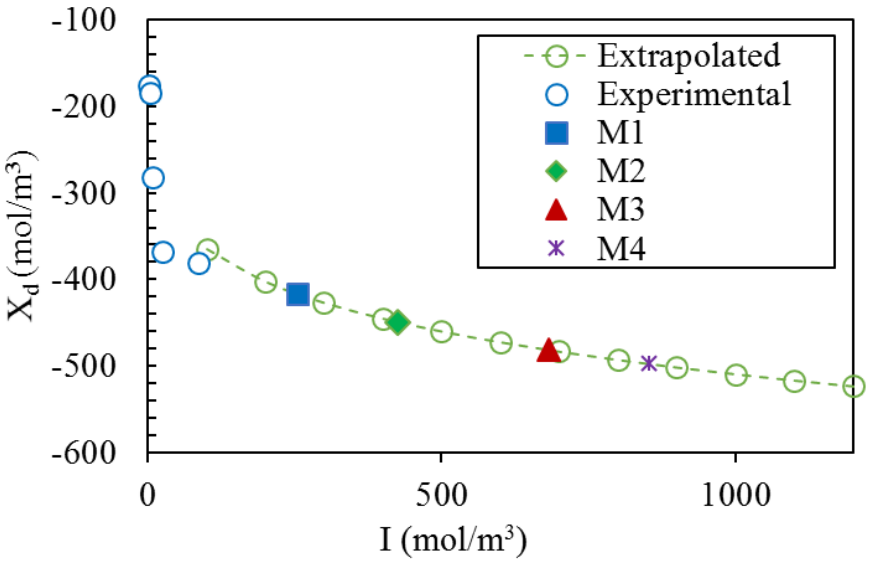

Figure 4. Effective charge density (X_d) values calculated from experimental ZP measurements and obtained from the extrapolation method. M1, M2, M3, and M4 refer to the model solutions that simulate the seawater RO concentrates.

As it is shown in Figure 4, the higher the ionic strength of the feed solution, the more negative the effective charge density becomes. Compared to the low range of ionic strength, there is a substantial change in the behaviour of the surface charge when high concentrations of salts are considered. The increase of effective charge density along ionic strength corresponds to the shielding of ions in the surface of the membrane and consequently the excess of counter-ions is neutralized.

Gouy-Chapman double layer theory predicts that the concentration of ions at the surface of the membrane can grow without limit, which is not coherent since the limitation is established by the size of these ions. This contradiction can be appreciated in Figure 4, which shows the variation of the membrane charge density with the ionic strength of the solution.

4.3. Simulation of ions rejection

Simulations of nanofiltration performance of NF270 for the chloride/sulfate separation were carried out for different operational pressures, using the DSPM model described in Table 1. Four synthetic solutions were prepared following the compositions reported by Pérez et al. [3,44], which corresponded with different chloride/sulfate molar ratios. Low chloride/sulfate ratio resembles the salinity composition found in the brines from inland brackish water desalination, while the high chloride/sulfate ratio is related to seawater reverse desalination brines composition. The model was implemented in the process simulator Aspen Custom Modeler (AspenTech). The effective charge density was determined through the methodology described in Section 4.2.

Table 3 collects the composition of the model brine solutions under study, the calculated ionic strength, and the effective surface charge density developed by the NF270 membrane, which was obtained following the procedure described above. The ratio of chloride to sulfate molar concentrations is also included, as the study is also focused on the analysis of the influence of sulfate concentration in the purification of chloride-rich desalination brines. The input data for the simulations were only the composition of the feed brines, and the results were shown as rejection percentage of the three ions under study Cl^-, SO_4^{2-} and Na^+.

Table 3. Compositions of saline solutions considered for ion rejection simulations with the calculated effective charge density for each feed solution.

Experiment	$[Cl^-]/[SO_4^{2-}]$	I (mol/m^3)	X_d (mol/m^3)
E1	1.7	375	-441.8
E2	5.1	654	-478.5
E3	10.2	1,055	-513.3
E4	13.6	1,247	-526.1

Ion rejections were calculated according to Eq. (29). Added to the simulated ion rejections (solid lines), comparison with the experimental values (symbols) reported by Perez-Gonzalez et al. [13], as a function of operational pressure is included in Figure 5.

$$\mathcal{R}_i = \left(1 - \frac{C_{Pi}}{C_{Ri}}\right)\cdot 100 \qquad (29)$$

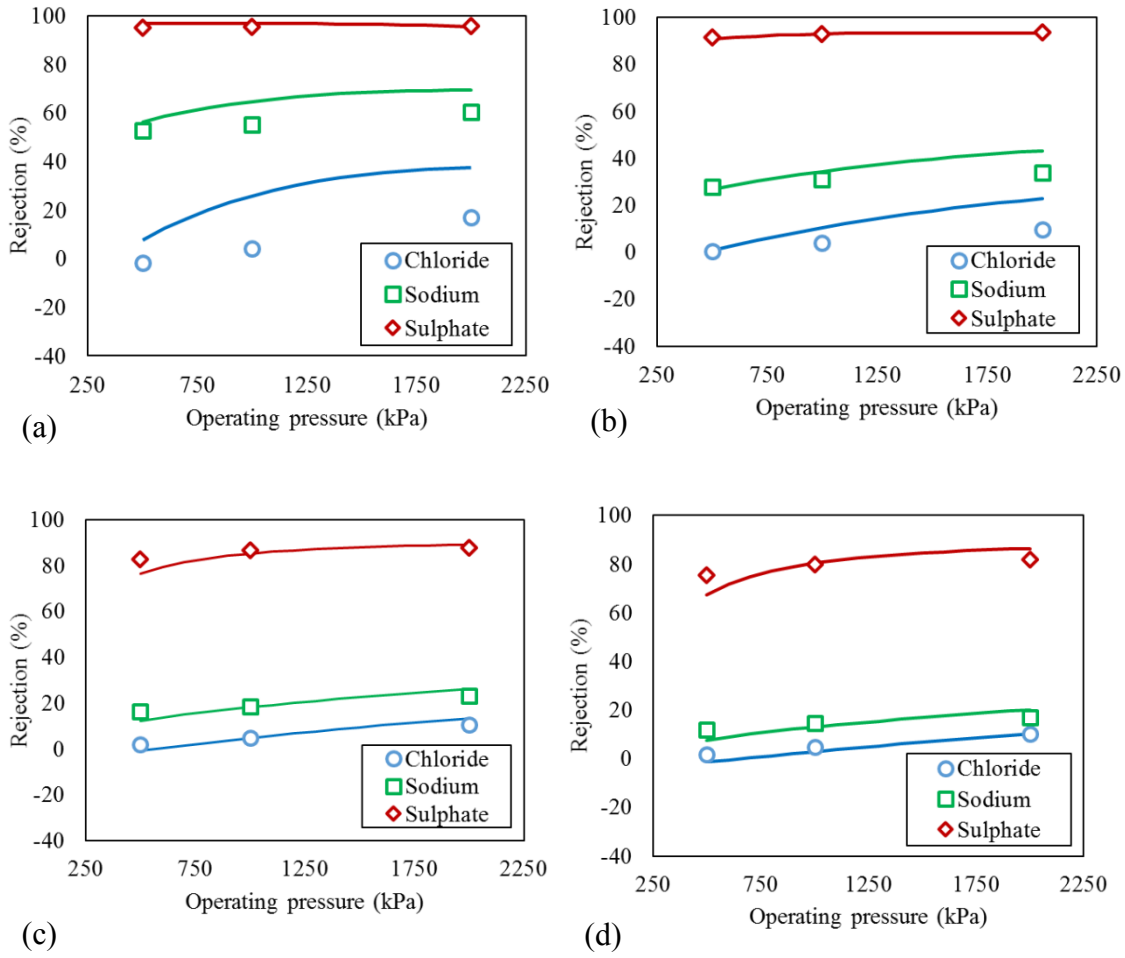

Figure 5. Ion rejections, NF270 membrane. Solid lines correspond to simulated values and symbols to the reported experimental values [3]. Each plot corresponds to one of the experimental conditions described in Table 3: (a) E1, (b) E2, (c) E3, and (d) E4.

Simulated results match to experimental data with good agreement. Simulations of sulfate rejections are particularly accurate for all the assayed mixtures, in the whole feed pressure range. Only for the lowest Cl^-/SO_4^{2-} ratio the model overestimates chloride rejections around 12% higher, a factor that also affects to the estimation of the sodium counter-ion. Simulation of sulfate rejection at any of the investigated conditions and of chloride rejection for Cl^-/SO_4^{2-} ratios ≥ 5.1 were in excellent agreement with the experimental data, with average standard deviation values of only 2%.

5. Conclusions

This work analyses the use of streaming potential measurements as a way to phenomenologically predict the performance of nanofiltration membranes for chloride and sulfate ions separation in the range of highly concentrated saline solutions, as those usually found in brackish water and seawater desalination brines. Particularly the prediction of the interfacial ion distribution phenomena occurring at charged nanofiltration membranes is studied.

This work adapted a methodology developed previously by Coday et al. [33] for forward osmosis applications, who related the streaming potential measurements with the Debye length, at low ionic concentrations, and extrapolated the obtained fitting to higher ionic strengths.

The application of the above referenced methodology enabled the description of the surface charge density developed by the NF270 membrane when working with several highly concentrated mixtures of chloride and sulfate anions, using sodium as common counter cation. The surface charged density vs. ionic strength correlation was incorporated to the Donnan steric pore model (DSPM) to simulate and predict the ion rejection performance obtained with the NF 270 membrane. The excellent correlation observed between the experimental and simulated results confirms the validity of the proposed approach. Therefore, an indirect method for the determination of effective charge density has been obtained and reported.

Acknowledgments

The authors gratefully acknowledge the funding for the projects CTM2016-75509-R and CTQ2015-66078-R

Nomenclature

A	membrane surface (m^2)
C	concentration (mol/m^3)
C_1	concentration in the membrane at the feed-membrane interface (mol/m^3)
C_2	concentration in the membrane at membrane-permeate interface (mol/m^3)
C_F	feed mole concentration (mol/m^3)

C_P	permeate mole concentration (mol/m^3)
C_R	retenate mole concentration (mol/m^3)
C_{eq}	Equivalent concentration (mol/m^3)
D_1	diffusivity of ions (m^2 ·s^{-1})
D_p	hindered diffusivity (m^2 ·s^{-1})
e	electronic charge (C)
F	Faraday constant (C/mol)
J_S	molar solute flux (mol·m^{-2}· s^{-1})
J_V	total volume flux (m·s^{-1})
k_B	Boltzmann constant (J/K)
k	conductivity of electrolyte solution (S/m)
K_c	convective hindrance factor, dimensionless
K_d	diffusive hindrance factor, dimensionless
L_p	solution membrane permeability (m·s^{-1} ·Pa^{-1})
L_{pw}	water membrane permeability (m·s^{-1} ·Pa^{-1})
Q_F	feed flow (m^3/s)
Q_P	permeate flow (m^3/s)
Q_R	retenate flow (m^3/s)
r_i	Stoke radius of ion (m)
r_p	effective pore radius (m)
$\mathcal{R}$	ion rejection, dimensionless
R	universal constant of gases (J·mol^{-1} ·K^{-1})
$R_{pressure}$	universal constant of gases (Pa·m^3 ·mol^{-1} ·K^{-1})
T	operation temperature (K)
T_f	solution fusion temperature (K)
T_f^*	water fusion temperature (K)
U	streaming potential (V)
V_{molar}	water molar volume (m^3/mol)
X_d	effective membrane charge density (mol/m^3)
z	ionic valence, dimensionless

Greek letters

α	ratio chloride concentration vs sulfate concentration
δ	thickness of the membrane effective layer (m)
ΔH_f^*	water fusion latent heat (J·mol^{-1})

$\Delta\pi$	osmotic pressure difference across the membrane (Pa)
ΔP	applied pressure difference across the membrane (Pa)
$\Delta\psi_{Donnan}$	Donnan potential, dimensionless
ε_0	vacuum permittivity (C/mV)
ε_r	dielectric constant of water, dimensionless
κ^{-1}	Debye length (m)
ξ	osmolality (mosmol·$(kg_{H2O})^{-1}$)
ζ	zeta potential (V)
λ	relative solute size, dimensionless
μ	solution viscosity (kg/ms)
σ_k	electrical charge on the membrane surface (C/m^2)
Φ	steric partitioning coefficient, dimensionless

Subscripts

i	ion
F	feed
P	permeate
R	retentate

References

[1] M.D. Afonso, G. Hagmeyer, R. Gimbel, Streaming potential measurements to assess the variation of nanofiltration membranes surface charge with the concentration of salt solutions, Sep. Purif. Technol. 2223 (2001) 529–541.

[2] M.R. Teixeira, M.J. Rosa, M. Nyström, The role of membrane charge on nanofiltration performance, J. Memb. Sci. 265 (2005) 160–166.

[3] A. Pérez-González, R. Ibáñez, P. Gómez, A.M. Urtiaga, I. Ortiz, J.A. Irabien, Nanofiltration separation of polyvalent and monovalent anions in desalination brines, J. Memb. Sci. 473 (2015) 16–27.

[4] M. Reig, N. Pagès, E. Licon, C. Valderrama, O. Gibert, A. Yaroshchuk, J.L. Cortina, Evolution of electrolyte mixtures rejection behaviour using nanofiltration membranes under spiral wound and flat-sheet configurations, Desalin. Water Treat. 56 (2015) 3519–3529.

[5] A. Lhassani, M. Rumeau, D. Benjelloun, M. Pontie, Selective demineralization of water by nanofiltration Application to the defluorination of brackish water, Water Res. 35 (2001) 3260–3264.

[6] A.S. Colburn, N. Meeks, S.T. Weinman, D. Bhattacharyya, High Total Dissolved Solids Water Treatment by Charged Nanofiltration Membranes Relating to Power Plant Applications, Ind. Eng. Chem. Res. 55 (2016) 4089–4097.

[7] Y. Liu, J. Wang, X. Sun, Energy-saving "NF/EDR" integrated membrane process for seawater desalination Part I. Seawater desalination by NF membrane with high desalination capacity, Desalination. 397 (2016) 165–173.

[8] S. Zhao, L. Zou, D. Mulcahy, Brackish water desalination by a hybrid forward osmosis–nanofiltration system using divalent draw solute, Desalination. 284 (2012) 175–181.

[9] N. Hilal, H. A1-Zoubp, N.A. Darwish, A.W. Mohammad, M.A. Arabi, A comprehensive review of nanofiltration membranes: Treatment, pretreatment, modelling, and atomic force microscopy, Desalination. 170 (2004) 281–308.

[10] A. Pérez-González, A.M. Urtiaga, R. Ibáñez, I. Ortiz, State of the art and review on the treatment technologies of water reverse osmosis concentrates, Water Res. 46 (2012) 267–283.

[11] C. Kaya, G. Sert, N. Kabay, M. Arda, M. Yüksel, Ö. Egemen, Pre-treatment with nanofiltration (NF) in seawater desalination—Preliminary integrated membrane tests in Urla, Turkey, Desalination. 369 (2015) 10–17.

[12] M. Reig, S. Casas, C. Aladjem, C. Valderrama, O. Gibert, F. Valero, C.M. Centeno, E. Larrotcha, J.L. Cortina, Concentration of NaCl from seawater reverse osmosis brines for the chlor-alkali industry by electrodialysis, Desalination. 342 (2014) 107–117.

[13] R. Ibáñez, A. Pérez-González, P. Gómez, A.M. Urtiaga, I. Ortiz, Acid and base recovery from softened reverse osmosis (RO) brines. Experimental assessment using model concentrates, Desalination. 309 (2013) 165–170.

[14] C. Fernandez-Gonzalez, A. Dominguez-Ramos, R. Ibañez, A. Irabien, Electrodialysis with Bipolar Membranes for Valorization of Brines, Sep. Purif.

Rev. 45 (2016) 275–287.

[15] C. Fernandez-Gonzalez, A. Dominguez-Ramos, R. Ibañez, Y. Chen, A. Irabien, Valorization of desalination brines by electrodialysis with bipolar membranes using nanocomposite anion exchange membranes, Desalination. 406 (2017) 16–24. doi:10.1016/j.desal.2016.07.033.

[16] M. Reig, S. Casas, O. Gibert, C. Valderrama, J.L. Cortina, Integration of nanofiltration and bipolar electrodialysis for valorization of seawater desalination brines: Production of drinking and waste water treatment chemicals, Desalination. 382 (2016) 13–20.

[17] G.H. Lopes, N. Ibaseta, P. Guichardon, How can osmosis and solute diffusion be coupled for the simultaneous measurement of the solvent and solute permeabilities of membranes?, Desalination. 387 (2016) 61–74.

[18] A.W. Mohammad, Y.H. Teow, W.L. Ang, Y.T. Chung, D.L. Oatley-Radcliffe, N. Hilal, Nanofiltration membranes review: Recent advances and future prospects, Desalination. 356 (2014) 226–254.

[19] W.R. Bowen, H. Mukhtar, Characterisation and prediction of separation performance of nanofiltration membranes, J. Memb. Sci. 112 (1996) 263–274.

[20] O. Agboola, J. Maree, R. Mbaya, Characterization and performance of nanofiltration membranes, Environ. Chem. Lett. 12 (2014) 241–255.

[21] K.S. Spiegler, O. Kedem, Thermodynamics of hyperfiltration (reverse osmosis): criteria for efficient membranes, Desalination. 1 (1966) 311–326.

[22] H. Al-Zoubi, N. Hilal, N.A. Darwish, A.W. Mohammad, Rejection and modelling of sulphate and potassium salts by nanofiltration membranes: neural network and Spiegler–Kedem model, Desalination. 206 (2007) 42–60.

[23] H. Al-Zoubi, W. Omar, Rejection of salt mixtures from high saline by nanofiltration membranes, Korean J. Chem. Eng. 26 (2009) 799–805.

[24] H. Al-Zoubi, W. Omar, Rejection of salt mixtures from high saline by nanofiltration membranes, Korean J. Chem. Eng. 26 (2009) 799–805.

[25] G. Artuğ, I. Roosmasari, K. Richau, J. Hapke, A Comprehensive Characterization

of Commercial Nanofiltration Membranes, Sep. Sci. Technol. 42 (2007) 2947–2986.

[26] D. Vezzani, S. Bandini, Donnan equilibrium and dielectric exclusion for characterization of nanofiltration membranes, Desalination. 149 (2002) 477–483.

[27] A. Szymczyk, P. Fievet, Investigating transport properties of nanofiltration membranes by means of a steric, electric and dielectric exclusion model, J. Memb. Sci. 252 (2005) 77–88.

[28] B. Saliha, F. Patrick, S. Anthony, Investigating nanofiltration of multi-ionic solutions using the steric, electric and dielectric exclusion model, Chem. Eng. Sci. 64 (2009) 3789–3798.

[29] K. Thibault, H. Zhu, A. Szymczyk, G. Li, The averaged potential gradient approach to model the rejection of electrolyte solutions using nanofiltration: Model development and assessment for highly concentrated feed solutions, Sep. Purif. Technol. 153 (2015) 126–137.

[30] W.R. Bowen, A.W. Mohammad, N. Hilal, Characterisation of nanofiltration membranes for predictive purposes - use of salts, uncharged solutes and atomic force microscopy, J. Memb. Sci. 126 (1997) 91–105.

[31] D.L. Oatley, L. Llenas, R. Pérez, P.M. Williams, X. Martínez-Lladó, M. Rovira, Review of the dielectric properties of nanofiltration membranes and verification of the single oriented layer approximation, Adv. Colloid Interface Sci. 173 (2012) 1–11.

[32] G. Hagmeyer, R. Gimbel, Modelling the rejection of nanofiltration membranes using zeta potential measurements, Sep. Purif. Technol. 15 (1999) 19–30.

[33] B.D. Coday, T. Luxbacher, A.E. Childress, N. Almaraz, P. Xu, T.Y. Cath, Indirect determination of zeta potential at high ionic strength: Specific application to semipermeable polymeric membranes, J. Memb. Sci. 478 (2015) 58–64.

[34] H. Buksek, T. Luxbacher, I. Petrinic, Zeta Potential Determination of Polymeric Materials Using Two Differently Designed Measuring Cells of an Electrokinetic Analyzer, Acta Chim. Slov. 57 (2010) 700–706.

[35] J. Luo, Y. Wan, Effects of pH and salt on nanofiltration-a critical review, J. Memb.

Sci. 438 (2013) 18–28.

[36] Y.-L. Lin, P.-C. Chiang, E.-E. Chang, Removal of small trihalomethane precursors from aqueous solution by nanofiltration., J. Hazard. Mater. 146 (2007) 20–9.

[37] W.R. Bowen, J.S. Welfoot, Modelling the performance of membrane nanofiltration—critical assessment and model development, Chem. Eng. Sci. 57 (2002) 1121–1137.

[38] L.D. Nghiem, A. Schäfer, M. Elimelech, Nanofiltration of hormone mimicking trace organic contaminants, Sep. Sci. Technol. 40 (2005) 2633–2649.

[39] N. Hilal, H. Al-Zoubi, A.W. Mohammad, N.A. Darwish, Nanofiltration of highly concentrated salt solutions up to seawater salinity, Desalination 184 (2005) 315–326.

[40] G. Hagmeyer, R. Gimbel, Modelling the rejection of nanofiltration membranes using zeta potential measurements, Sep. Purif. Technol. 15 (1999) 19–30.

[41] V. Freger, Swelling and Morphology of the Skin Layer of Polyamide Composite Membranes: An Atomic Force Microscopy Study, Environ. Sci. Technol. 38 (2004) 3168–3175.

[42] X.-L. Wang, T. Tsuru, S. Nakao, S. Kimura, The electrostatic and steric-hindrance model for the transport of charged solutes through nanofiltration membranes, J. Memb. Sci. 135 (1997) 19–32.

[43] J.M.M. Peeters, M.H.V. Mulder, H. Strathmann, Streaming potential measurements as a characterization method for nanofiltration membranes, Colloids Surfaces A Physicochem. Eng. Asp. 150 (1999) 247–259.

[44] A. Pérez-González, R. Ibáñez, P. Gómez, A. Urtiaga, I. Ortiz, Integration of nanofiltration for the sustainable management of reverse osmosis brines, Chem. Eng. Trans. 39 (2014) 85–90.

[45] J. Schaep, C. Vandecasteele, Evaluating the charge of nanofiltration membranes, J. Memb. Sci. 188 (2001) 129–136.

[46] E. Idil Mouhoumed, A. Szymczyk, A. Schäfer, L. Paugam, Y.H. La, Physico-chemical characterization of polyamide NF/RO membranes: Insight from

streaming current measurements, J. Memb. Sci. 461 (2014) 130–138.

[47] S. Bandini, Modelling the mechanism of charge formation in NF membranes: Theory and application, J. Memb. Sci. 264 (2005) 75–86.

[48] G. Bargeman, J.B. Westerink, C.F.H. Manuhutu, A. ten Kate, The effect of membrane characteristics on nanofiltration membrane performance during processing of practically saturated salt solutions, J. Memb. Sci. 485 (2015) 112–122.

[49] K. Boussu, Y. Zhang, J. Cocquyt, P. Van der Meeren, A. Volodin, C. Van Haesendonck, J.A. Martens, B. Van der Bruggen, Characterization of polymeric nanofiltration membranes for systematic analysis of membrane performance, J. Memb. Sci. 278 (2006) 418–427.

[50] A.E. Childress, M. Elimelech, Effect of solution chemistry on the surface charge of polymeric reverse osmosis and nanofiltration membranes, J. Memb. Sci. 119 (1996) 253–268.

[51] J.H. Tay, J. Liu, D. Delai Sun, Effect of solution physico-chemistry on the charge property of nanofiltration membranes, Water Res. 36 (2002) 585–598.

[52] J. Lyklema, Chapter 3. Electric double layers, in: Fundam. Interface Colloid Sci. Solid-Liquid Interface, Academic Press, San Diego, 1995.

[53] Á. Soriano, D. Gorri, A. Urtiaga, Efficient treatment of perfluorohexanoic acid by nanofiltration followed by electrochemical degradation of the NF concentrate, Water Res. 112 (2017) 147–156.

[54] A. Pérez-González, R. Ibáñez, P. Gómez, A.M. Urtiaga, I. Ortiz, J.A. Irabien, Recovery of desalination brines: separation of calcium, magnesium and sulfate as a pre-treatment step, Desalin. Water Treat. 56 (2015) 3617–3625.

[55] A. Yaroshchuk, T. Luxbacher, Interpretation of electrokinetic measurements with porous films: Role of electric conductance and streaming current within porous structure, Langmuir. 26 (2010) 10882–10889.

[56] A.J.C. Semião, A.I. Schäfer, Estrogenic micropollutant adsorption dynamics onto nanofiltration membranes, J. Memb. Sci. 381 (2011) 132–141.

[57] C.Y. Tang, Y.-N. Kwon, J.O. Leckie, Characterization of Humic Acid Fouled Reverse Osmosis and Nanofiltration Membranes by Transmission Electron Microscopy and Streaming Potential Measurements, Environ. Sci. Technol. 41 (2007) 942–949.

[58] B.E. Conway, Ionic Hydration in Chemistry and Biophysics, 1st Editio, Elvesier Science, Amsterdam and New York, 1982.